J Control Theory Appl 2008 6 (1) 59–68
DOI 10.1007/s11768-008-7193-9

A novel induction motor control scheme using IDA-PBC

Humberto GONZÁLEZ [1], Manuel A. DUARTE-MERMOUD [1], Ian PELISSIER [1],
Juan Carlos TRAVIESO-TORRES [1], Romeo ORTEGA [2]

(1.Department of Electrical Engineering, University of Chile, Casilla 412-3, Santiago, Chile;

2.Laboratoire des Signaux et Systèmes, Plateau de Moulon 91192, Gif-sur-Yvette, France)

Abstract: A new control scheme for induction motors is proposed in the present paper, applying the interconnection and damping assignment-passivity based control (IDA-PBC) method. The scheme is based exclusively on passivity based control, without restricting the input frequency as it is done in field oriented control (FOC). A port-controlled Hamiltonian (PCH) model of the induction motor is deduced to make the interconnection and damping of energy explicit on the scheme. The proposed controller is validated under computational simulations and experimental tests using an inverter prototype.

Keywords: Induction motor; Passivity based control; Energy shaping control; Interconnection and damping assignment; IDA-PBC; Port-controlled Hamiltonian; PCH

1 Introduction

Passivity-based control (PBC) has become an important tool in nonlinear control research, mainly because of its straightforward application to physical systems (mechanical, electrical and electromechanical). In recent years, interconnection and damping assignment-passivity based control (IDA-PBC) has appeared as a flexible and versatile method to design controllers for nonlinear systems, introducing tools to assign the interconnection and damping of internal energy.

Also, induction motors are an interesting area of research for nonlinear control [1, 2]. Their wider use replacing DC motors has been an incentive to develop more and better techniques to control their dynamic behavior to obtain a more efficient use of the energy without losing performance.

The present paper analyzes the use of IDA-PBC as a method to control induction motors. The result is a new scheme to design controllers for induction motors focusing on energy characteristics, like equilibrium and shape, to achieve the desired objective. This result does not use field oriented control (FOC) or any other scheme to fix the input voltage frequency; on the contrary, the input frequency is used as a fundamental part of the solution. As a result of the new scheme, a speed regulator is obtained and simulated with an induction motor model in the Matlab-Simulink environment. To apply the IDA-PBC method to induction motors, a port-controlled Hamiltonian (PCH) model is deducted for the complete electro-mechanical system. Also, using an inverter prototype designed in [3], a set of experiments are performed showing the behavior of the proposed scheme.

This IDA-PBC controller is based on a different paradigm for the induction motor control than the one used in FOC. Instead of decoupling the inputs of the induction motor to make it similar to a DC motor, the IDA-PBC controller takes advantage of the internal properties of the system to reach the desired objective without intermediate steps.

2 IDA-PBC control

2.1 Passive systems

The definition of a passive system is taken from [4]. Other ways to state this definition, using the concept of dissipative systems, can be found in [5].

Definition 1 [4] Let Σ_p be a dynamical system,

$$\Sigma_p : \begin{cases} \dot{x} = f(x) + g(x)u, \\ y = h(x) \end{cases} \tag{1}$$

with $u, y \in \mathbb{R}^p$, $x \in X \subseteq \mathbb{R}^n$ and an equilibrium point $x^* \in X$ such that $f(x^*) = 0$ and $h(x^*) = 0$. This system will be called passive if there is a continuous function $H : X \to \mathbb{R}^+$ with $H(x^*) = 0$, called the storage function, such that $\forall t \geqslant t_0 \in \mathbb{R}$ and $\forall u(\cdot)$

$$H(x(t)) - H(x(t_0)) \leqslant \int_{t_0}^{t} u^{\mathrm{T}}(s)y(s)\mathrm{d}s. \tag{2}$$

The function $H(\cdot)$ is related with the stored energy of a system and, in a consistent way, the product $u^{\mathrm{T}}(t)y(t)$ has instant power units. The inequality (2) shows that the internal stored energy of a passive system is always less than or equal to the energy supplied to it, or in other words, a pas-

Received 22 October 2007.
This work was supported by CONICYT Chile through grant FONDECYT (1061170).

sive system is unable to generate energy. The relation (2) is called Dissipation Inequality.

2.2 PCH models

An interesting point of view in modeling dynamical systems has been raised following the known methodologies of Lagrange and Hamilton, because they generate equations with structures that allow to establish physical relationships based on their variables and parameters. Particularly, we will analyze the systems modeled with the Hamilton equations. A deeper study on this issues is found on [5∼8].

Definition 2 [5] A dynamical system $\Sigma_{\rm PCH}$ has a PCH model if its mathematic representation has the form,

$$\Sigma_{\rm PCH}: \begin{cases} \dot{x} = [\mathcal{J}(x) - \mathcal{R}(x)]\nabla H + g(x)u, \\ y = g^{\rm T}(x)\nabla H, \end{cases} \tag{3}$$

where

- $H(x): \mathbb{R}^n \to \mathbb{R}$ is a $\mathcal{C}^1$ function that represents the internal energy in the system.
- $x \in \mathbb{R}^n$ are the state variables.
- $\mathcal{J}(x) = -\mathcal{J}^{\rm T}(x)$ is the interconnection matrix.
- $\mathcal{R}(x) = \mathcal{R}(x) \geqslant 0$ is the damping matrix.
- $g(x)$ is the input matrix.

The close relationship between the physical phenomenon and its PCH model is the main contribution of this representation, because it allows a direct read of the internal interconnection and damping of energy on the matrices $\mathcal{J}$ and $\mathcal{R}$. This reason makes the PCH models particulary suitable to analyze electrical, mechanical or electromechanical systems, because the physical knowledge is used to understand their behaviour.

Moreover, it is proved in [5] that if $H(\cdot)$ is bounded from below, then the system $\Sigma_{\rm PCH}$ is passive, with $H(\cdot)$ as the storage function.

2.3 IDA-PBC control

The interconnection and damping assignment-passivity-based control (IDA-PBC), when used on PCH models, can assign the interconnection, damping and internal energy of a closed loop by changing the matrices $\mathcal{J}$, $\mathcal{R}$ and the storage function H. The formulation for general models of systems is found in [9, 10].

Theorem 1 Let $\Sigma_{\rm PCH}$ be a system described by the equation (3). Let us assume that there are matrices $g^{\perp}(x)$, $\mathcal{J}_{\rm d} = -\mathcal{J}_{\rm d}^{\rm T}$, $\mathcal{R}_{\rm d} = \mathcal{R}_{\rm d}^{\rm T} \geqslant 0$ and a function $H_{\rm d}: \mathbb{R}^n \to \mathbb{R}$ such that

$$g^{\perp}[\mathcal{J} - \mathcal{R}]\nabla H = g^{\perp}[\mathcal{J}_{\rm d} - \mathcal{R}_{\rm d}]\nabla H_{\rm d}, \tag{4}$$

where $g^{\perp}(x)$ is a full range left-annihilator of $g(x)$, i.e., $g^{\perp}g = 0$, and $H_{\rm d}$ such that

$$x^* = \arg\min_{x\in\mathbb{R}^n} H_{\rm d}(x). \tag{5}$$

Then, applying the control $u = \beta(x)$, where

$$\beta = \begin{bmatrix} g^{\rm T} \\ g \end{bmatrix}^{-1} g^{\rm T}\left\{[\mathcal{J}_{\rm d} - \mathcal{R}_{\rm d}]\nabla H_{\rm d} - [\mathcal{J} - \mathcal{R}]\nabla H\right\}, \tag{6}$$

the closed-loop dynamics will be

$$\dot{x} = [\mathcal{J}_{\rm d} - \mathcal{R}_{\rm d}]\nabla H_{\rm d} \tag{7}$$

with x^* as a locally stable equilibrium point in the Lyapunov sense. The equilibrium point will be asymptotically stable in the Lyapunov sense if the largest invariant set contained in

$$\left\{x \in \mathbb{R}^n \,\middle|\, \nabla H_{\rm d}^{\rm T}(x)\mathcal{R}_{\rm d}(x)\nabla H_{\rm d}(x)\right\} \tag{8}$$

equals $\{x^*\}$.

A complete demonstration of the previous theorem can be found in [10].

3 Induction motor: PCH model and IDA-PBC control

The deduction of the PCH model for an induction motor will be divided in two parts: the electrical subsystem model and the mechanical subsystem model.

3.1 Electrical subsystem

The general equations for AC machines are used to study this subsystem, as they are commonly used in [11, 12] to analyze triphase motors.

Under symmetry hypothesis of the coils in the motor, and using the Voltage Kirchhoff law over stator and rotor circuits, the equations are

$$u_{\rm s} = R_{\rm s}i_{\rm s} + \frac{{\rm d}\psi_{\rm s}}{{\rm d}t}, \tag{9a}$$

$$0 = R_{\rm r}i_{\rm r} + \frac{{\rm d}\psi_{\rm r}}{{\rm d}t}, \tag{9b}$$

with $u_{\rm s}$ being the voltage applied to the stator, $i_{\rm s}$ and $i_{\rm r}$ the stator and rotor currents respectively, $\psi_{\rm s}$ and $\psi_{\rm r}$ the magnetic fluxes linked by the stator and rotor coils, and $R_{\rm s}$ and $R_{\rm r}$ the stator and rotor internal resistance, respectively. In addition, the magnetic coupling between stator and rotor is modeled as

$$\psi_{\rm s} = L_{\rm s}i_{\rm s} + L_{\rm m}i_{\rm r}, \;\; \psi_{\rm r} = L_{\rm m}i_{\rm s} + L_{\rm r}i_{\rm r}, \tag{10}$$

where $L_{\rm s}$ and $L_{\rm r}$ are the stator and rotor self-inductances, and $L_{\rm m}$ is the mutual-inductance between both circuits.

Let a new reference frame rotated ρ_g radians with respect to the stator frame, as shown in Fig.1.

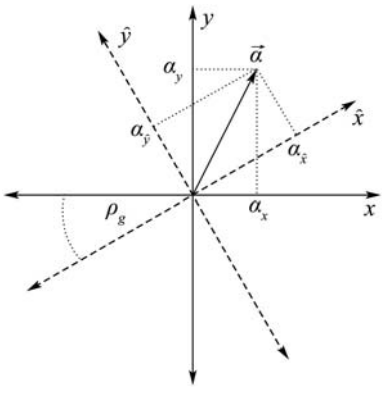

Fig. 1 Phasor diagram of the reference frame rotated ρ_g radians.

In this new system, the equation (9a) is transformed to

$$\begin{aligned} u_{\rm s} &= R_{\rm s}{\rm e}^{j\rho_g} i_{{\rm s}g} + \frac{{\rm d}({\rm e}^{j\rho_g}\psi_{{\rm s}g})}{{\rm d}t} \\ &= R_{\rm s}{\rm e}^{j\rho_g} i_{{\rm s}g} + {\rm e}^{j\rho_g}\frac{{\rm d}\psi_{{\rm s}g}}{{\rm d}t} + j{\rm e}^{j\rho_g}\omega_g\psi_{{\rm s}g}, \end{aligned} \quad (11)$$

where ω_g is the temporal derivative of ρ_g, i.e., the angular velocity of the reference frame. In addition, if the voltage applied to $u_{{\rm s}g}$ is defined as $u_{\rm s} = {\rm e}^{j\rho_g}u_{{\rm s}g}$ then, using (11), we get

$$u_{{\rm s}g} = R_{\rm s} i_{{\rm s}g} + \frac{{\rm d}\psi_{{\rm s}g}}{{\rm d}t} + j\omega_g\psi_{{\rm s}g}. \quad (12)$$

Let $\theta_{\rm r}$ be the rotor mechanical angle. Then, using a reference frame rotated $(\rho_g - \theta_{\rm r})$ radians, the equation (9b) implies

$$\begin{aligned} 0 &= R_{\rm r}{\rm e}^{j(\rho_g-\theta_{\rm r})} i_{{\rm r}g} + {\rm e}^{j(\rho_g-\theta_{\rm r})}\frac{{\rm d}\psi_{{\rm r}g}}{{\rm d}t} \\ &\quad + j{\rm e}^{j(\rho_g-\theta_{\rm r})}(\omega_g - \omega_{\rm r})\psi_{{\rm r}g} \\ &= R_{\rm r} i_{{\rm r}g} + \frac{{\rm d}\psi_{{\rm r}g}}{{\rm d}t} + j(\omega_g - \omega_{\rm r})\psi_{{\rm r}g}, \end{aligned} \quad (13)$$

where $\omega_{\rm r}$ is the temporal derivative of $\theta_{\rm r}$, i.e., the rotor angular velocity.

Defining the real and imaginary parts of the following variables:

$$\begin{cases} u_{{\rm s}g} = u_{{\rm s}x} + ju_{{\rm s}y}, \\ i_{{\rm s}g} = i_{{\rm s}x} + ji_{{\rm s}y}, \\ i_{{\rm r}g} = i_{{\rm r}x} + ji_{{\rm r}y}, \\ \psi_{{\rm s}g} = \psi_{{\rm s}x} + j\psi_{{\rm s}y}, \\ \psi_{{\rm r}g} = \psi_{{\rm r}x} + j\psi_{{\rm r}y}, \end{cases} \quad (14)$$

equations (12) and (13) are equivalent to

$$\begin{cases} u_{{\rm s}x} = R_{\rm s} i_{{\rm s}x} + \dot{\psi}_{{\rm s}x} - \omega_g\psi_{{\rm s}y}, \\ 0 = R_{\rm r} i_{{\rm r}x} + \dot{\psi}_{{\rm r}x} - (\omega_g - \omega_{\rm r})\psi_{{\rm r}y}, \\ u_{{\rm s}y} = R_{\rm s} i_{{\rm s}y} + \dot{\psi}_{{\rm s}y} + \omega_g\psi_{{\rm s}x}, \\ 0 = R_{\rm r} i_{{\rm r}y} + \dot{\psi}_{{\rm r}y} + (\omega_g - \omega_{\rm r})\psi_{{\rm r}x}. \end{cases} \quad (15)$$

Using (10) and organizing the terms, these equations are transformed to

$$\begin{cases} \dot{\psi}_{{\rm s}x} = -R_{\rm s} i_{{\rm s}x} + \omega_g L_{\rm s} i_{{\rm s}y} + \omega_g L_{\rm m} i_{{\rm r}y} + u_{{\rm s}x}, \\ \dot{\psi}_{{\rm r}x} = -R_{\rm r} i_{{\rm r}x} + \omega_g L_{\rm m} i_{{\rm s}y} + \omega_g L_{\rm r} i_{{\rm r}y} - \omega_{\rm r}\psi_{{\rm r}y}, \\ \dot{\psi}_{{\rm s}y} = -R_{\rm s} i_{{\rm s}y} - \omega_g L_{\rm s} i_{{\rm s}x} - \omega_g L_{\rm m} i_{{\rm r}x} + u_{{\rm s}y}, \\ \dot{\psi}_{{\rm r}y} = -R_{\rm r} i_{{\rm r}y} - \omega_g L_{\rm m} i_{{\rm s}x} - \omega_g L_{\rm r} i_{{\rm r}x} + \omega_{\rm r}\psi_{{\rm r}x} \end{cases} \quad (16)$$

or

$$\begin{cases} \dot{\psi}_x = -Ri_x + \omega_g L i_y - \begin{bmatrix} 0 \\ \psi_{{\rm r}y} \end{bmatrix}\omega_{\rm r} + \begin{bmatrix} u_{{\rm s}x} \\ 0 \end{bmatrix}, \\ \dot{\psi}_y = -Ri_y - \omega_g L i_x + \begin{bmatrix} 0 \\ \psi_{{\rm r}x} \end{bmatrix}\omega_{\rm r} + \begin{bmatrix} u_{{\rm s}y} \\ 0 \end{bmatrix} \end{cases} \quad (17)$$

with

$$\begin{cases} \psi_x = \begin{bmatrix} \psi_{{\rm s}x} \\ \psi_{{\rm r}x} \end{bmatrix},\ \psi_y = \begin{bmatrix} \psi_{{\rm s}y} \\ \psi_{{\rm r}y} \end{bmatrix},\ i_x = \begin{bmatrix} i_{{\rm s}x} \\ i_{{\rm r}x} \end{bmatrix},\ i_y = \begin{bmatrix} i_{{\rm s}y} \\ i_{{\rm r}y} \end{bmatrix}, \\ R = \begin{bmatrix} R_{\rm s} & 0 \\ 0 & R_{\rm r} \end{bmatrix},\ L = \begin{bmatrix} L_{\rm s} & L_{\rm m} \\ L_{\rm m} & L_{\rm r} \end{bmatrix}. \end{cases} \quad (18)$$

3.2 Mechanical subsystem

Applying the second Newton law in the rotor axis, the following equation is obtained:

$$J\dot{\omega}_{\rm r} = -B_p\omega_{\rm r} + T_{\rm EM} - T_{\rm L} \quad (19)$$

with J being the rotor inertial momentum, B_p the friction coefficient of the rotor, $T_{\rm EM}$ the electromagnetical torque generated by the electrical subsystem and $T_{\rm L}$ the load torque applied to the rotor.

The electromagnetical torque is modeled in [11] as

$$\begin{aligned} T_{\rm EM} &= L_{\rm m} i_{\rm r} \times i_{\rm s} = L_{\rm m}\left(i_{{\rm s}y} i_{{\rm r}x} - i_{{\rm s}x} i_{{\rm r}y}\right) \\ &= \psi_{{\rm r}y} i_{{\rm r}x} - \psi_{{\rm r}x} i_{{\rm r}y} \end{aligned} \quad (20)$$

and the equation (19) becomes

$$J\dot{\omega}_{\rm r} = -B_p\omega_{\rm r} + \psi_{{\rm r}y} i_{{\rm r}x} - \psi_{{\rm r}x} i_{{\rm r}y} - T_{\rm L}. \quad (21)$$

3.3 System energy and PCH model

Defining the state variables as

$$x = \begin{bmatrix} \psi_{{\rm s}x} & \psi_{{\rm r}x} & \psi_{{\rm s}y} & \psi_{{\rm r}y} & J\omega_{\rm r} \end{bmatrix}^{\rm T} = \begin{bmatrix} \psi_x^{\rm T} & \psi_y^{\rm T} & J\omega_{\rm r} \end{bmatrix}^{\rm T} \in \mathbb{R}^5, \quad (22)$$

hence the system's energy H, which is formed by the magnetic energy of the coils and the kinetic energy of the rotor, is written in terms of the state variables as

$$H = \frac{1}{2}x_{12}^{\rm T} L^{-1} x_{12} + \frac{1}{2}x_{34}^{\rm T} L^{-1} x_{34} + \frac{1}{2}J^{-1}x_5^2, \quad (23)$$

where

$$x_{12} = \psi_x = [\psi_{{\rm s}x} \ \ \psi_{{\rm r}x}]^{\rm T},\ x_{34} = \psi_y = [\psi_{{\rm s}y} \ \ \psi_{{\rm r}y}]^{\rm T}.$$

The partial derivatives of the energy with respect to the state variables are

$$\begin{cases} \dfrac{\partial H}{\partial x_{12}} = L^{-1}x_{12} = i_x \Rightarrow \begin{cases} \dfrac{\partial H}{\partial x_1} = i_{{\rm s}x}, \\ \dfrac{\partial H}{\partial x_2} = i_{{\rm r}x}, \end{cases} \\ \dfrac{\partial H}{\partial x_{34}} = L^{-1}x_{34} = i_y \Rightarrow \begin{cases} \dfrac{\partial H}{\partial x_3} = i_{{\rm s}y}, \\ \dfrac{\partial H}{\partial x_4} = i_{{\rm r}y}, \end{cases} \\ \dfrac{\partial H}{\partial x_5} = J^{-1}x_5 = \omega_{\rm r}. \end{cases} \quad (24)$$

If the angular velocity of the reference system ω_g is fixed to the voltage electrical frequency $\omega_{\rm s}$ then its value can be arbitrarily assigned, which means that it can be used as a new input for our model. Also, as a simplification to the mechanical subsystem, the load torque applied to the axis will be considered to be in the following form:

$$T_{\rm L} = B\omega_{\rm r} \quad (25)$$

with B being a positive constant value.

Using the electrical and mechanical equations shown in (17) and (21), which are written based on the state variables (22), and applying the simplifications for the angular velocity of the reference frame ω_g and the load torque $T_{\rm L}$ (in the equation (25)), the following equations are obtained as the induction motor model

$$\begin{cases} \dot{x} = \begin{bmatrix} -R_{\rm s} & 0 & 0 & 0 & 0 \\ 0 & -R_{\rm r} & 0 & 0 & -x_4 \\ 0 & 0 & -R_{\rm s} & 0 & 0 \\ 0 & 0 & 0 & -R_{\rm r} & x_2 \\ 0 & x_4 & 0 & -x_2 & -B' \end{bmatrix} \nabla H \\ \qquad + \begin{bmatrix} 1 & 0 & x_3 \\ 0 & 0 & x_4 \\ 0 & 1 & -x_1 \\ 0 & 0 & -x_2 \\ 0 & 0 & 0 \end{bmatrix} \begin{bmatrix} u_{sx} \\ u_{sy} \\ \omega_{\rm s} \end{bmatrix}, \\ y = \begin{bmatrix} 1 & 0 & 0 & 0 & 0 \\ 0 & 0 & 1 & 0 & 0 \\ x_3 & x_4 & -x_1 & -x_2 & 0 \end{bmatrix} \nabla H = \begin{bmatrix} i_{sx} \\ i_{sy} \\ 0 \end{bmatrix}, \end{cases} \tag{26}$$

where $B' = B_p + B$. The third element of the output vector is used to maintain the mathematical framework of passivity, where the product between $u(t)$ and $y(t)$ has instant power units. In physical terms, the new input $\omega_{\rm s}$ is not involved with power delivery, so it must be multiplied by zero.

The following matrices can be identified from the system in the equation (26)

$$\begin{cases} \mathcal{J}(x) = \begin{bmatrix} 0 & 0 & 0 & 0 & 0 \\ 0 & 0 & 0 & 0 & -x_4 \\ 0 & 0 & 0 & 0 & 0 \\ 0 & 0 & 0 & 0 & x_2 \\ 0 & x_4 & 0 & -x_2 & 0 \end{bmatrix}, \\ \mathcal{R}(x) = \begin{bmatrix} R_{\rm s} & 0 & 0 & 0 & 0 \\ 0 & R_{\rm r} & 0 & 0 & 0 \\ 0 & 0 & R_{\rm s} & 0 & 0 \\ 0 & 0 & 0 & R_{\rm r} & 0 \\ 0 & 0 & 0 & 0 & B' \end{bmatrix}, \\ g(x) = \begin{bmatrix} 1 & 0 & x_3 \\ 0 & 0 & x_4 \\ 0 & 1 & -x_1 \\ 0 & 0 & -x_2 \\ 0 & 0 & 0 \end{bmatrix}, \end{cases} \tag{27}$$

where $\mathcal{J} = -\mathcal{J}^{\rm T}$ and $\mathcal{R} = \mathcal{R}^{\rm T} \geqslant 0$. With these matrices, the system (26) can be written as a PCH model

$$\dot{x} = [\mathcal{J} - \mathcal{R}]\nabla H + gu, \;\; y = g^{\rm T}\nabla H, \tag{28}$$

where $u = [u_{sx} \;\; u_{sy} \;\; \omega_{\rm s}]^{\rm T} \in \mathbb{R}^3$ are the inputs of the system. Also, as the energy H is bounded from below, the PCH model is passive.

3.4 Control

To apply the IDA-PBC control, the matrices $\mathcal{J}_{\rm d}$, $\mathcal{R}_{\rm d}$ and $g^{\perp}$ are chosen as

$$\begin{cases} \mathcal{J}_{\rm d}(x) = \mathcal{J}(x), \; \mathcal{R}_{\rm d}(x) = \mathcal{R}(x), \\ g^{\perp}(x) = \begin{bmatrix} 0 & 0 & 0 & 0 & 1 \\ 0 & x_2 & 0 & x_4 & 0 \end{bmatrix}, \end{cases} \tag{29}$$

where $\mathcal{J}$ and $\mathcal{R}$ are the matrices shown in equation (27). With these matrices, the PDE (4) can be simplified as

$$g^{\perp}[\mathcal{J} - \mathcal{R}]\nabla H_{\rm a} = 0 \tag{30}$$

with $H_{\rm a}$ being the energy applied by the controller, and therefore the energy of the closed loop is $H_{\rm d} = H + H_{\rm a}$. After evaluating $g^{\perp}$, $\mathcal{J}$ and $\mathcal{R}$, the following two equations are obtained:

$$\begin{cases} x_2\left[-R_{\rm r}\dfrac{\partial H_{\rm a}}{\partial x_2} - x_4\dfrac{\partial H_{\rm a}}{\partial x_5}\right] + x_4\left[-R_{\rm r}\dfrac{\partial H_{\rm a}}{\partial x_4} + x_2\dfrac{\partial H_{\rm a}}{\partial x_5}\right] \\ \quad = 0, \\ x_4\dfrac{\partial H_{\rm a}}{\partial x_2} - x_2\dfrac{\partial H_{\rm a}}{\partial x_4} - B'\dfrac{\partial H_{\rm a}}{\partial x_5} = 0 \end{cases} \tag{31}$$

with a general solution

$$H_{\rm a} = H_{\rm a}\left(x_1, x_3, x_5 + B'\arctan\left(\frac{x_2}{x_4}\right)\right). \tag{32}$$

Once the solution to the equation system (31) is obtained, a suitable function $H_{\rm a}$ must be selected. This means that the selected function must fix the equilibrium point to reach the desired steady state response of the system and at the same time must define the transient response using the "geometrical shape" of the energy.

Since the objective of this controller is to regulate the angular velocity $\omega_{\rm r}$, the chosen applied energy function is

$$H_{\rm a} = k_1x_1 + k_2x_3 + k_3\left[x_5 + B'\arctan\left(\frac{x_2}{x_4}\right)\right] \tag{33}$$

with $k_i, \; i = 1, 2, 3$ real constant values. The equilibrium points of the closed loop are defined by the solutions to $\nabla(H + H_{\rm a}) = 0$:

$$L^{-1}x_{12} + \begin{bmatrix} k_1 \\ \dfrac{x_4}{x_2^2 + x_4^2}k_3B' \end{bmatrix} = 0, \tag{34a}$$

$$L^{-1}x_{34} + \begin{bmatrix} k_2 \\ -\dfrac{x_2}{x_2^2 + x_4^2}k_3B' \end{bmatrix} = 0, \tag{34b}$$

$$J^{-1}x_5 + k_3 = 0. \tag{34c}$$

It can be easily deduced from the equation (34c) that the angular velocity $\omega_{\rm r}$ has a unique equilibrium point in $\omega_{\rm r}^* = -k_3$, which validates this controller as an angular speed regulator for induction motors. The general solution to the equations is shown in the Appendix, including the

equilibrium points of all the electrical state variables.

Finally, the control that must be applied is given by the equation (6) and has the form

$$u_{sx}(x) = -R_{\rm s}k_1 + \left(1 + \frac{R_{\rm r}B'}{x_2^2 + x_4^2}\right) x_3 k_3, \quad (35a)$$

$$u_{sy}(x) = -R_{\rm s}k_2 - \left(1 + \frac{R_{\rm r}B'}{x_2^2 + x_4^2}\right) x_1 k_3, \quad (35b)$$

$$\omega_{\rm s}(x) = -\left(1 + \frac{R_{\rm r}B'}{x_2^2 + x_4^2}\right) k_3, \quad (35c)$$

where $k_3 = -\omega_{\rm r}^*$ and the constants k_1 and k_2 are chosen to give an equilibrium point to every state variable in the equation's system (34) (in Appendix, it is shown that not every value of k_1 and k_2 solves the equation system).

To implement this controller in a real motor, the stator and rotor magnetic fluxes must be known at every instant of time. This issue can be surpassed by using a magnetic flux observer for the motor, taking the estimated measures as replacements of the unknown state variables. A complete review in this area can be found in [16].

4 Simulation results

A simulation of the previous scheme was built using Matlab-Simulink. The parameters used in the model of the motor are shown in Table 1, which are the same values used in [13]

Table 1 Parameters used in the PCH induction motor model.

Parameter	Value
$R_{\rm s}$	$0.687\ \Omega$
$R_{\rm r}$	$0.842\ \Omega$
$L_{\rm s}$	84 mH
$L_{\rm r}$	85.2 mH
$L_{\rm m}$	81.3 mH
B_p	$0.01\ \mathrm{Kg}\cdot\mathrm{m}^2/\mathrm{s}$
B	$0\ \mathrm{Kg}\cdot\mathrm{m}^2/\mathrm{s}$
J	$0.03\ \mathrm{Kg}\cdot\mathrm{m}^2/\mathrm{s}$

The initial conditions and the controller parameters were chosen as

$$\begin{cases} x_0 = [0\ \ 0.1\ \ 0\ \ 0.1\ \ 0]^{\rm T}, \\ k_1 = -5,\ k_2 = -10,\ k_3 = -50. \end{cases} \quad (36)$$

Using the parameter values included in Table 1, the values of the constants k_1, k_2 and k_3, and the general solution to the equation system (34) included in Appendix, the equilibrium points of the closed loop are

$$\begin{cases} x_{\varepsilon 1} = [0.45896\ \ 0.44734\ \ 0.81794\ \ 0.78988\ \ 1.5]^{\rm T}, \\ x_{\varepsilon 2} = [0.07314\ \ 0.043\ \ 0.04628\ \ -0.0188\ \ 1.5]^{\rm T}. \end{cases} \quad (37)$$

A linearized model of the closed loop over each of these equilibrium points was used to analyze their stability. The poles of the system linearized over $x = x_{\varepsilon 1}$ are

$$\begin{cases} \lambda_{11} = -212.13,\ \lambda_{12} = -231.7, \\ \lambda_{13} = -12.241 + 3.843\,\mathrm{j},\ \lambda_{14} = -12.241 - 3.843\,\mathrm{j}, \\ \lambda_{15} = -4.5409 \end{cases} \quad (38)$$

and the poles of the closed loop system linearized over $x = x_{\varepsilon 2}$ are

$$\begin{cases} \lambda_{21} = -369.12,\ \lambda_{22} = 118.56,\ \lambda_{23} = -163.62, \\ \lambda_{24} = -58.257,\ \lambda_{25} = -0.4205, \end{cases} \quad (39)$$

hence, as the closed loop system is asymptotically stable and the equilibrium point $x_{\varepsilon 2}$ has a pole with positive real part, the state will converge to $x_{\varepsilon 1}$ as the time goes to infinity.

The results of the simulation defined by the previous parameters are shown in Figs.2 to 5. Notice that the amplitudes of the electrical variables (input voltages and motor currents) are kept under acceptable bounds in terms of real motor nominal values. The controller does not try to cancel the nonlinear behavior of the system but uses it to achieve the control objective.

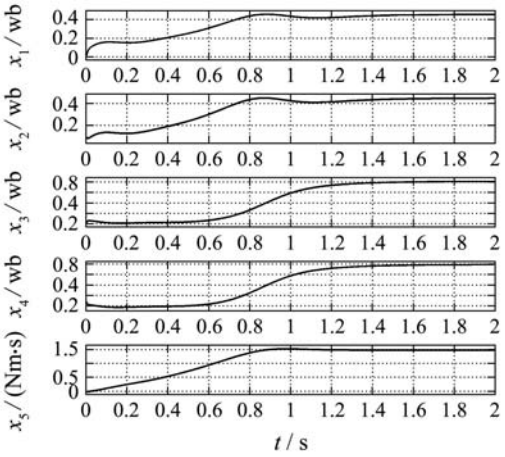

Fig. 2 Time evolution of the internal state variables.

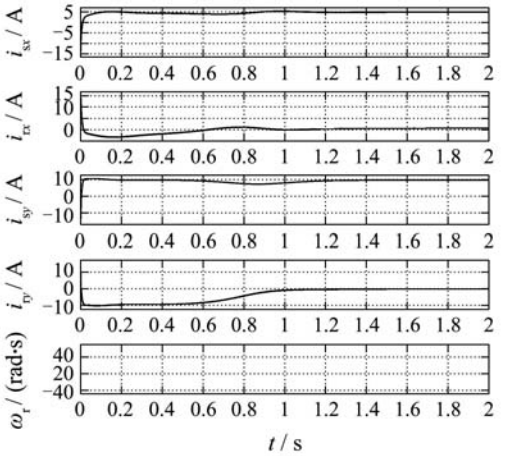

Fig. 3 Time evolution of the motor currents (stator and rotor) and the angular velocity.

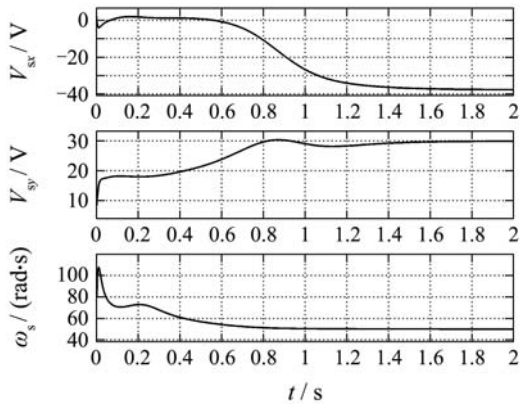

Fig. 4 Time evolution of the inputs to the system: voltages and frequency.

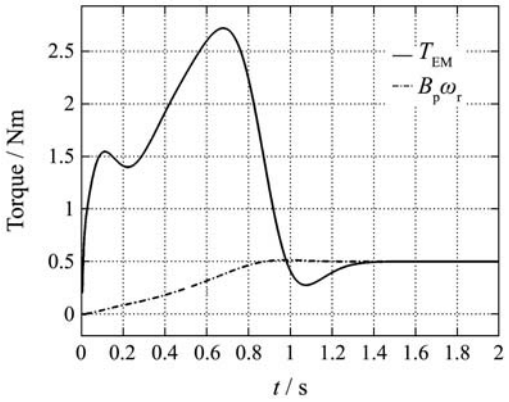

Fig. 5 Time evolution of the electromagnetic torque vs. the load torque.

5 Experimental results

For the IDA-PBC scheme used in this paper, it is necessary to introduce some modifications to obtain experimental results. In principle, this strategy was developed to control the mechanical speed of the motor, being unable to control mechanical torque perturbations. This implies that permanent errors in the mechanical speed are obtained, in simulations as well as in experiments. To solve this problem, a simple proportional integral (PI) controller loop was added in the original scheme for the mechanical speed reference, as shown in Fig.6.

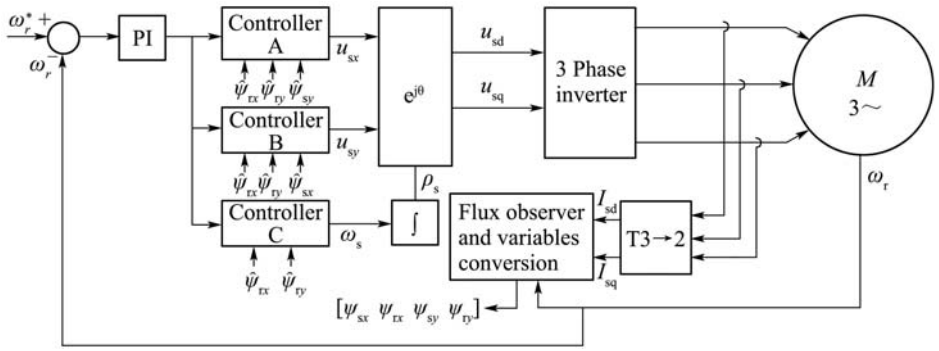

Fig. 6 Modified IDA-PBC control scheme.

In the case of the induction motor, the rotor flux cannot be measured directly, so the implementation of a rotor flux observer becomes necessary in order to implement the IDA-PBC scheme. The observer used in this study was implemented based on the voltage-current model of the induction motor, which is developed in [14∼16] and it is shown next.

The current model of the induction motor is given by

$$\dot{\hat{\psi}}_{\mathrm{dqr}} = \frac{\hat{R}_{\mathrm{r}} L_{\mathrm{m}}}{L_{\mathrm{r}}} i_{\mathrm{dqr}} - \hat{\omega}_{\mathrm{r}} \hat{\psi}_{\mathrm{dqr}}, \tag{40}$$

where $\hat{\omega}_{\mathrm{r}} = \hat{R}_{\mathrm{r}}/L_{\mathrm{r}} - \omega_{\mathrm{r}}\mathrm{j}$ and $\hat{R}_{\mathrm{r}}$ represents the rotor resistance estimation of the observer. Then, considering only variations on rotor resistance, the relationship between the observed flux and the real one is

$$\frac{\hat{\psi}_{\mathrm{dqr}}}{\psi_{\mathrm{dqr}}} = \frac{\hat{R}_{\mathrm{r}}(s+\hat{\omega}_{\mathrm{r}})}{R_{\mathrm{r}}(s+\omega_{\mathrm{r}})} = FRF_{\mathrm{c}}. \tag{41}$$

On the other hand, the open loop voltage model is

$$\dot{\hat{\psi}}_{\mathrm{dqs}} = v_{\mathrm{dqs}} - \hat{R}_{\mathrm{s}} i_{\mathrm{dqs}}, \tag{42}$$

where $\hat{\psi}_{\mathrm{dqr}} = \dfrac{L_{\mathrm{r}}}{L_{\mathrm{m}}}\hat{\psi}_{\mathrm{dqs}} - \dfrac{\sigma}{1-\sigma} L_{\mathrm{m}} i_{\mathrm{dqs}}$. The transfer function between the observed flux and the real one for the voltage model is

$$\frac{\hat{\psi}_{\mathrm{dqr}}}{\psi_{\mathrm{dqr}}} = 1 + \frac{L_{\mathrm{r}}^2}{R_{\mathrm{r}} L_{\mathrm{m}}^2}\left(\frac{s+\omega_{\mathrm{r}}}{s}\right)(R_{\mathrm{s}} - \hat{R}_{\mathrm{s}}) = FRF_{\mathrm{v}}. \tag{43}$$

It is important to point out that the current model gives a good estimate at low speeds and the voltage model gives a good estimate at high speeds. To be able to use both models, they are grouped using a transition function of the form $K(s) = k_1 + k_2/s$. Then, the following transfer function is obtained:

$$\frac{\hat{\psi}_{\mathrm{dqr}}}{\psi_{\mathrm{dqr}}} = \frac{\frac{L_{\mathrm{m}}}{L_{\mathrm{r}}} s(FRF_{\mathrm{v}}) + K(FRF_{\mathrm{c}})}{\frac{L_{\mathrm{m}}}{L_{\mathrm{r}}} s + K}. \tag{44}$$

With the transfer function shown above, a rotor flux observer is obtained for the induction motor, which considers the rotor resistance variations. Because of the form of the observer, its formulation is only valid when the mechanical speed, ω_{r}, is constant or varies slowly since otherwise the term $\hat{\omega}_{\mathrm{r}}\hat{\psi}_{\mathrm{dq}}$ adds a non considered dynamics into the model.

The experimental results are obtained using a 3ϕ inverter developed in [3] which communicates to the PC using the software Matlab-Simulink with an S-Function. The

induction motor used was a Siemens 1LA7080, 0.55KW, $\cos\phi$=0.82, 220V, 2.5A, 4 poles and 1395rpm. The motor was tested to obtain its electrical parameters, which are given in Table 2.

Table 2 Induction motor parameters.

Parameter	$R_{\rm s}$	$R_{\rm r}$	$X_{\rm s}$	$X_{\rm r}$	$X_{\rm m}$
Value(Ω)	14.7	5.5184	11.5655	11.5655	115.3113

To apply mechanical load to the induction motor, it was mechanically coupled to a continuous current generator, Briggs and Stratton ETEK, with permanent magnets, making it ideal to use as an electric generator. The load of the generator was applied to the stator using a cage of discrete resistances, controlled manually by switches, allowing with this to apply resistive torque onto the rotor axis of the induction motor. The experimental assembly consisting of the motor-generator group used in the experimental tests is shown in Fig.7:

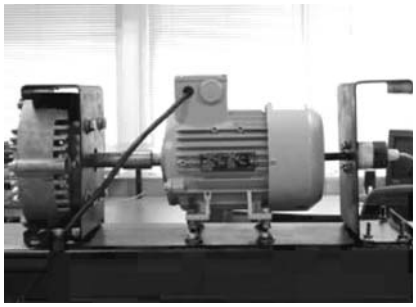

Fig. 7 Experimental assembly.

The constant values k_1 and k_2 were chosen by performing preliminary tests, obtaining the values $k_1 = k_2 = -30$ and for the proportional integral loop it was obtained $K_{_P} = 3$ and $K_{_I} = 0.5$. The tests carried out on the induction motor are the following:

· Test 1: Speed reference of ramp type from zero to nominal value in 9 seconds. Load torque proportional to the speed equals to the nominal value (100%) during the whole test.

· Test 2: Speed reference of ramp type from zero to nominal value in 9 seconds. Between $t = 40$s and $t = 70$s the reference is a pulse train of amplitude $0.1\omega_{\rm r_{nom}}$ and frequency $2\pi/20$. Between $t = 80$s and $t = 110$s the reference is sinusoidal of amplitude $0.1\omega_{\rm r_{nom}}$ and frequency $2\pi/20$. Load torque proportional to the speed equals to 50% of the nominal value during the whole test.

· Test 3: Speed reference of ramp type from zero to nominal value in 9 seconds. Initial load torque equals to 0% of the nominal value. Between $t = 40$s and $t = 80$s a torque perturbation equal to 50% of the nominal value is added.

The results of the experimental tests are shown in Figs.8 to 10. The blue line in the first subfigure is the speed reference and the green line is the measured mechanical speed. In the third subfigure, the blue line is the stator RMS voltage applied to the motor, and the green line is the frequency (in Hz) of the RMS voltage.

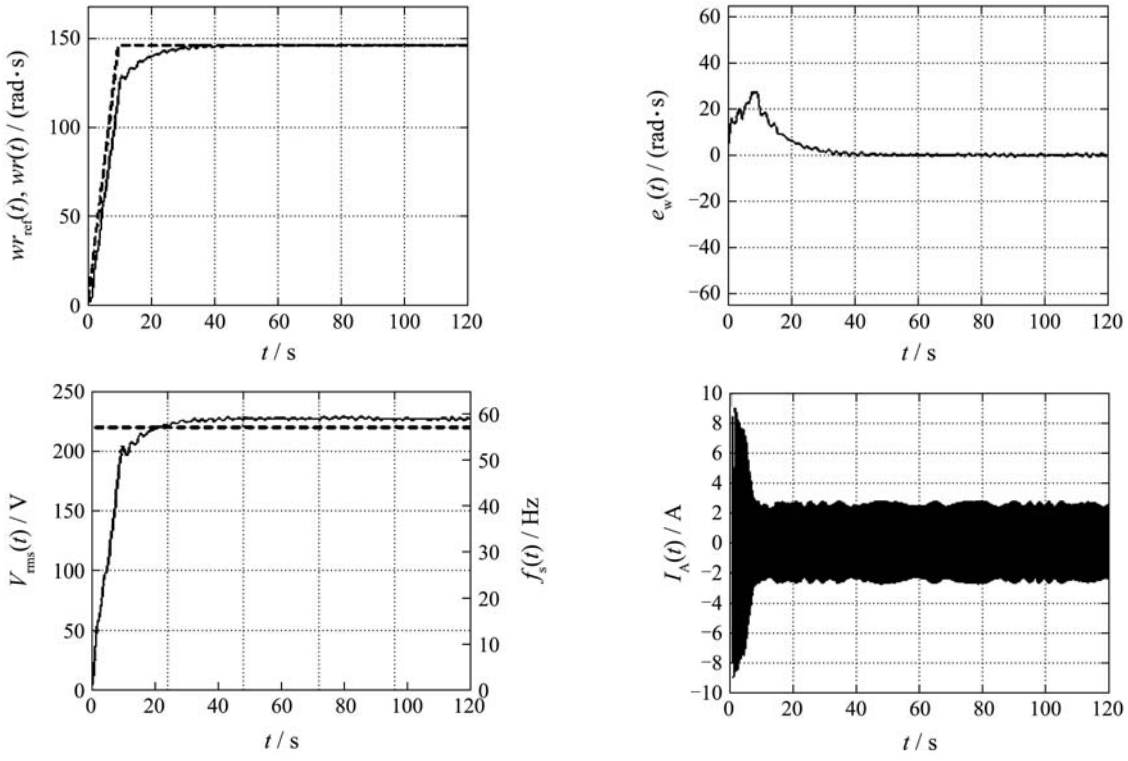

Fig. 8 Experimental results test 1.

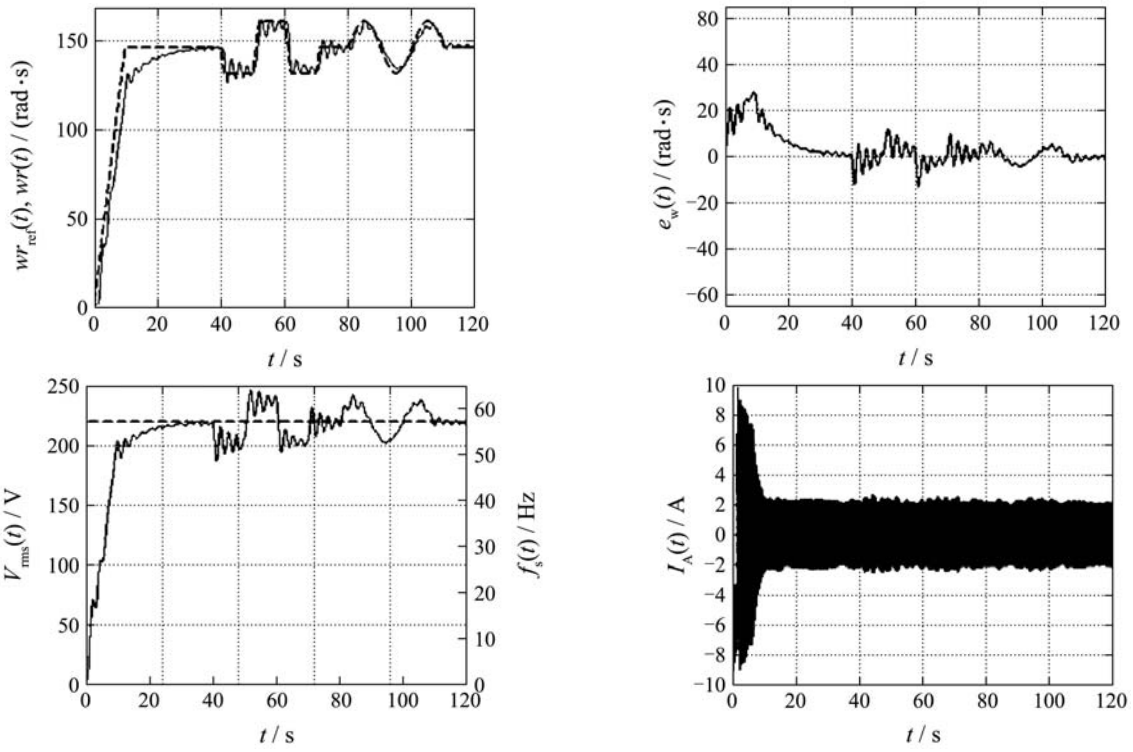

Fig. 9 Experimental results test 2.

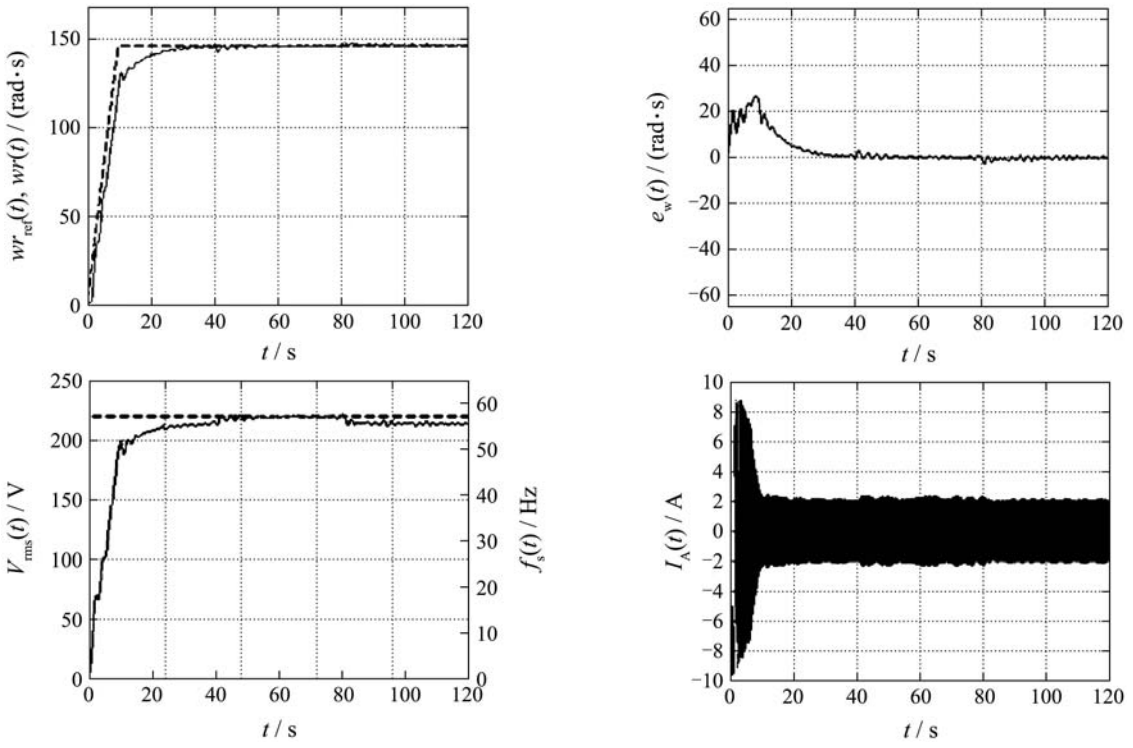

Fig. 10 Experimental results test 3.

As shown in the results, an oscillatory component appears in the signal due to the dynamics of the flux observer, which is valid only when the mechanical speed varies slowly. Thus, when a speed ramp reference is applied, the observer oscillates until the speed is stabilized. These oscillations are also because we are not considering the variations induced by the addition of the proportional integral outer loop in the formulation of the IDA-PBC scheme.

6 Conclusions

A novel scheme was presented to control an induction motor based on the energy shape of the system. This scheme

allows to choose the closed loop energy shape, and the electrical variables are a consequence of this choice. One of the main characteristics of this scheme is that the concept of Field Oriented Control is not needed, giving more freedom when designing a control scheme for induction motors. It is shown that the scheme achieved the control objectives in simulations as well as in experiments.

Acknowledgements

The authors wish to thank CONICYT Chile, through grant FONDECYT 1061170, for the support in developing this work.

References

[1] R. Ortega, G. Espinoza-Pérez. Passivity-based control with simultaneous energy-shaping and damping injection: the induction motor case study[C]*//Proceedings of the 16th IFAC World Congress*. Prague: Elsevier Science, 2005.

[2] D. Karagiannis, R. Ortega, A. Astolfi, et al. A nonlinear tracking controller for voltage-fed induction motors with uncertain load torque[J]. *IEEE Transactions on Control Systems Technology*, 2008 (in press).

[3] H. González. *Development of Control Schemes Based on Energy Shaping for A Class of Nonlinear Systems and Design of A Triphase Inverter Open Prototype for Online Applications in Induction Motors*[D]. Santiago: University of Chile, 2005 (in Spanish).

[4] C. I. CByrnes, A. Isidori, J. C.Willems. Passivity, feedback equivalence, and the global stabilization of minimum phase nonlinear systems[J]. *IEEE Transactions on Automatic Control*, 1991, 36(11): 1228 – 1240.

[5] A. van der Schaft. *L_2-Gain and Passivity Techniques in Nonlinear Control*[M]. 2nd ed. Berlin: Springer-Verlag, 2000.

[6] B. M. Maschke, A. J. van der Schaft, P. C. Breedveld. An intrinsic Hamiltonian formulation of network dynamics: non-standard Poisson structures and gyrators[J]. *Journal of the Franklin Institute*, 1992, 329(5): 923 – 966.

[7] R. Ortega, A. Loria, P. J. Nicklasson, et al. *Passivity-Based Control of Euler-Lagrange Systems*[M]. New York: Springer-Verlag, 1998.

[8] R. Ortega, M. W. Spong. Adaptive motion control of rigid robots: a tutorial[J]. *Automatica*. 1998, 25(6): 877 – 888.

[9] R. Ortega, E. Garcĺa-Canseco. Interconnection and damping assignment passivity-based control: a survey[J]. *European Journal of Control*. 2004, 10(5): 432 – 450.

[10] R. Ortega, A. van der Schaft, B. Maschke, et al. Interconnection and damping assignment passivity-based control of port-controlled Hamiltonian systems[J]. *Automatica*. 2002, 38(4): 585 – 596.

[11] B. Adkins, R. G. Harley. *The General Theory of Alternating Current Machines: Application to Practical Problems*[M]. London: Chapman and Hall, 1975.

[12] P. Vas. *Electrical Machines and Drives: A Space-Vector Theory Approach*[M]. Oxford: Clarendon Press, 1992.

[13] R. Ortega, G. Espinoza. Torque regulation of induction motors[J]. *Automatica*, 1993, 29(3): 621 – 633.

[14] P. L. Jansen, R. D. Lorenz. A physically insightful approach to the design and accuracyassessment of flux observers for field oriented induction machine drives[J]. *IEEE Transactions on Industrial Applications*, 1994, 30(1): 101 – 110.

[15] P. L. Jansen, C. Thompson, R. D. Lorenz. Observer-based direct field orientation for both zero and very high speed operation[C]*// Conference Record of the Power Conversion Conference - Yokohama*. New York: IEEE Press, 1993: 432 – 437.

[16] C. Martín. *Comparative Analysis of Magnetic Flux Observers for Induction Motor Control Schemes*[D]. Santiago: University of Chile, 2005 (in Spanish).

Appendix

A1 Solution of the equilibrium point equation system

The complete solution of the equation system (34) is shown in equations (a1) to (a5).

$$x_1=\frac{1}{\Delta}\Big\{2k_1k_2k_3B\Big[\left(k_1^2+k_2^2\right)\left(-L_{\rm s}L_{\rm r}+L_{\rm m}^2\right)+\xi\Big] +k_1^2\left(k_1^2+k_2^2\right)\left(-L_{\rm s}+\frac{L_{\rm m}^2}{L_{\rm r}}\right)\Big[\left(k_1^2+k_2^2\right)L_{\rm m}^2+\xi\Big] +2k_3^2L_{\rm r}B^2\left(k_2^2-k_1^2\right)\Big\}, \tag{a1}$$

$$x_2=\frac{2k_3L_{\rm r}B}{L_{\rm m}\Delta}\Big[k_3L_{\rm r}B\left(k_2^2-k_1^2\right)+k_1k_2\xi\Big], \tag{a2}$$

$$x_3=-L_{\rm s}k_2+\frac{1}{2\left(k_1^2+k_2^2\right)L_{\rm r}}\Big\{-2k_1k_3L_{\rm r}B +k_2\left[\left(k_1^2+k_2^2\right)L_{\rm m}^2+\xi\right]\Big\}, \tag{a3}$$

$$x_4=\frac{1}{2\left(k_1^2+k_2^2\right)L_{\rm m}}\Big\{-2k_1k_3L_{\rm r}B -k_2\left[\left(k_1^2+k_2^2\right)L_{\rm m}^2+\xi\right]\Big\}, \tag{a4}$$

$$x_5=-k_3J, \tag{a5}$$

where

$$\Delta=\left(k_1^2+k_2^2\right)\Big\{2k_2k_3L_{\rm r}B+k_1\left[\left(k_1^2+k_2^2\right)L_{\rm m}^2+\xi\right]\Big\}, \tag{a6}$$

$$\xi=\pm\sqrt{\left(k_1^2+k_2^2\right)^2L_{\rm m}^4-4k_3^2L_{\rm r}^2B^2}. \tag{a7}$$

Thus, the variables ξ and Δ define the existence and number of solutions. There will be no solutions only if:

$$\Delta=0\vee\left(k_1^2+k_2^2\right)L_{\rm m}^2<2k_3L_{\rm r}B, \tag{a8}$$

also, given $\Delta\neq0$, there will be one solution if

$$\left(k_1^2+k_2^2\right)L_{\rm m}^2=2k_3L_{\rm r}B, \tag{a9}$$

and two solutions if

$$\left(k_1^2+k_2^2\right)L_{\rm m}^2>2k_3L_{\rm r}B. \tag{a10}$$

Humberto GONÁLEZ was born in Chile in 1981. He received the B.S. and M.S. degrees in electrical engineering from the University of Chile, in 2005. Currently, he is a graduate student in the Department of Electrical Engineering and Computer Sciences at University of California, Berkeley. His research interests are in nonlinear and hybrid control. E-mail: hgonzale@EECS.Berkeley.EDU.

Manuel A. DUARTE-MERMOUD received the degree of Civil Electrical Engineer from the University of Chile in 1977 and the M.Sc., M.Phil. and the Ph.D. degrees, all in electrical engineering, from Yale University in 1985, 1986 and 1988, respectively. From 1977 to 1979, he worked as Field Engineer at Santiago Subway. In 1979 he joined the Electrical Engineering Department of University of Chile, where he is currently Professor. His main research interests are in robust adaptive control (linear and nonlinear systems) and system identification. He is member of the IEEE and IFAC. He is past Treasurer and past President of ACCA, the Chilean National Member Organization of IFAC, and past Vice-President of the IEEE-Chile. E-mail: mduartem@ing.uchile.cl.

Ian PELISSIER was born in Chile in 1981. He received the B.S. degree in electrical engineering from the University of Chile, in 2006. Currently, he is a research engineer in the department of Electrical Engineering of University of Chile working on improvement of the bio-leaching and electro-winning copper operations using heating by electromagnetic induction. His research interests are in electrical machines control. E-mail: ipelissi@ing.uchile.cl.

Juan Carlos TRAVIESO-TORRES was born in 1973, receiving the degrees of Electrical Engineer and M.Sc. from the Superior Polytechnic Institute "José Antonio Echeverría" at Havana, Cuba, in 1995 and 2000, respectively; and the Ph.D. degree at the University of Santiago of Chile in 2003. He has more than eleven years of professional experience working for different companies, and more than seven years of teaching and research experience at the Electrical Engineering Departments of the University of Santiago of Chile, and at the University of Chile. He was considered by Fluor Corporation a global expert in the subjects of DCS/PLC, Process Control, and Variable Speed Drives which are his main research areas. E-mail: jtravies@ing.uchile.cl.

Romeo ORTEGA was born in Mexico. He obtained his B.S. in Electrical and Mechanical Engineering from the National University of Mexico, Mexico, Master of Engineering from Polytechnical Institute of Leningrad, USSR, and the Docteur D'Etat from the Polytechnical Institute of Grenoble, France in 1974, 1978 and 1984, respectively. Currently he is in the Laboratoire de Signaux ET Systemes of Supelec in Gif-sur-Yvette, France, where he holds a position of Directeur de Recherche from the CNRS. His research interests are in the fields of nonlinear and adaptive control with special emphasis on applications. E-mail: Romeo.Ortega@lss.supelec.fr.